ISSN 1674-1056
http://cpb.iphy.ac.cn
http://iopscience.iop.org/cpb
中国物理 B
Chinese Physics
中国物理
Chinese Physics B

Modified physical optics algorithm for near field scattering

Bin Chen(陈彬), Chuangming Tong(童创明)

Citation: Chin. Phys. B . 2018, 27(11): 114102. **doi:** 10.1088/1674-1056/27/114102
Journal homepage: http://cpb.iphy.ac.cn; http://iopscience.iop.org/cpb

What follows is a list of articles you may be interested in

Studies on convergence and scaling law of Thomson backscattering spectra in strong fields

Han-Zhang Xie(谢含章), Chun Jiang(蒋纯), Bai-Song Xie(谢柏松)
Chin. Phys. B . 2017, 26(12): 124101. **doi:** 10.1088/1674-1056/26/12/124101

Effective dielectric constant model of electromagnetic backscattering from stratified air-sea surface film-sea water medium

Tao Xie(谢涛), William Perrie, He Fang(方贺), Li Zhao(赵立), Wen-Jin Yu(于文金), Yi-Jun He(何宜军)
Chin. Phys. B . 2017, 26(5): 054102. **doi:** 10.1088/1674-1056/26/5/054102

Electromagnetic backscattering from one-dimensional drifting fractal sea surface II:Electromagnetic backscattering model

Tao Xie(谢涛), William Perrie, Shang-Zhuo Zhao(赵尚卓), He Fang(方贺), Wen-Jin Yu(于文金), Yi-Jun He(何宜军)
Chin. Phys. B . 2016, 25(7): 074102. **doi:** 10.1088/1674-1056/25/7/074102

The polarization effect of a laser in multiphoton Compton scattering

Liang Guo-Hua, Lü Qing-Zheng, Teng Ai-Ping, Li Ying-Jun
Chin. Phys. B . 2014, 23(5): 054103. **doi:** 10.1088/1674-1056/23/5/054103

Numerical simulation for all-optical Thomson scattering X-ray source

Tan Fang, Zhu Bin, Han Dan, Xin Jian-Ting, Zhao Zong-Qing, Cao Lei-Feng, Gu Yu-Qiu, Zhang Bao-Han
Chin. Phys. B . 2014, 23(3): 034104. **doi:** 10.1088/1674-1056/23/3/034104

Modified physical optics algorithm for near field scattering

Bin Chen(陈彬)† and Chuangming Tong(童创明)

Air Force Engineering University, Xi'an 710051, *China*

(Received 21 May 2018; revised manuscript received 10 July 2018; published online 19 October 2018)

A novel modified physical optics algorithm is proposed to overcome the difficulties of near field scattering prediction for classical physical optics. The method is applied to calculating the near field radar cross section of electrically large objects by taking into account the influence of the distinct wave propagation vector, the near field Green function, and the antenna radiation pattern. By setting up local reference coordinates, each partitioned facet has its own distinct wave front curvature. The radiation gain for every surface element is taken into consideration based on the modulation of the antenna radiation pattern. The Green function is refined both in amplitude and phase terms and allows for near field calculation. The scattered characteristics of the near field targets are studied by numerical simulations. The results show that the approach can achieve a satisfactory accuracy.

Keywords: physical optics, scattering, near field

PACS: 41.20.–q **DOI:** 10.1088/1674-1056/27/11/114102

1. Introduction

Significant challenges still exist in estimating the radar characteristics of a complex electrically large target using numerical evaluation methods, despite constant development in computational capabilities and algorithms. Physical optics (PO), relying on assumptions attuned to large scale problems, has been widely adopted with efficiency and accuracy to estimate the radar cross sections (RCS) of electrically large targets. An important assumption in the simplification of the PO method is that the observation point should be far away from the source. As the standard PO code is usually optimized in far field conditions, it cannot be applied directly to the evaluation of near field scattering due to the finite distance between the source and observer.

In recent years, to overcome the shortcomings of PO in the near field zone, several approaches have been used to modify the standard PO for near field calculations. The physical theory of diffraction and the method of shooting and bouncing rays were modified with a spherical wave by Jeng for near field computation.[1] A near field RCS calculation method with exact Green function was introduced by Neto[2] and Chen *et al.*[3] The accuracy of this algorithm is excellent, but the efficiency is undesirable for electrically large targets due to the requirement for numerical integration of the surface currents. An approach proposed by Legault overcomes this difficulty by means of locally expanded phase approximations combined with surface partitioning.[4] Papkelis *et al.* derived an accurate and time-efficient analytical PO method for near field calculation of rectangular plates.[5] The near field formulation of PO and equivalent edge currents was developed in Refs. [6] and [7] by introducing the concept of the distinct wave propagation vector. A PO near field refinement was introduced in Ref. [8] for dielectric and perfect electric conducting (PEC) targets. In Refs. [9] and [10], a near field fast PO algorithm for large convex objects was presented, using phase and amplitude compensation factors. In Ref. [11], the influence of the antenna and distance as well as spherical wave irradiation was taken into account in near field calculation. A computational method of near field RCS was proposed using the surface element as the calculating unit by Cheng.[12,13]

In this work, we propose a modified physical optics (MPO) algorithm for the analysis of complex electrically large targets with PEC surface in the near field zone. The differences between the incident wave and antenna radiation pattern in either the near or far range are taken into consideration. A more accurate representation of the Green function in the near field is also employed in this algorithm. The proposed algorithm can be seen as a near field extension of the standard PO based on the principles presented in Refs. [3] and [5]. Each meshed facet is treated as an individual object. Every single facet has its own incident wave expressed with a spherical wave front and radiation gain described by the antenna radiation pattern. Furthermore, the far field assumption is replaced by a more accurate phase approximation of the Green function to overcome the shortcomings of the standard PO in the near field. The formulation of MPO is derived on the basis of the proposed principle and applied to discuss near field scattering characteristics. This algorithm preserves the simplicity of refined PO in Ref. [3] and is more accurate than the method in Ref. [5].

This paper is arranged as follows. In Section 2, the assumptions in the far field are introduced. The near field modifications in physical optics are derived in detail in Section 3. In Section 4, the accuracy of the presented algorithm and the near field characteristics of the targets are discussed via several nu-

†Corresponding author. E-mail: chin_cem@126.com

© 2018 Chinese Physical Society and IOP Publishing Ltd

merical examples. Section 5 concludes the current work and looks forward to future work.

2. Assumptions in the far field

According to the electric field integral equation (EFIE), the scattered field $\boldsymbol{E}_{\rm s}(\boldsymbol{r})$ for an electrically large PEC object of maximum dimension D with surface S and surface normal $\hat{\boldsymbol{n}}$, is given by[14]

$$\begin{aligned}\boldsymbol{E}_{\rm s}(\boldsymbol{r}) = & \int_{S_{\rm lit}} \left[{\rm j}\omega\mu\left(\hat{\boldsymbol{n}}\times\boldsymbol{H}\right)\psi_0+\left(\hat{\boldsymbol{n}}\times\boldsymbol{E}\right)\right.\\ & \left.\times\nabla\psi_0+\left(\hat{\boldsymbol{n}}\cdot\boldsymbol{E}\right)\nabla\psi_0\right]{\rm d}S\\ & +\frac{1}{{\rm j}\omega\varepsilon}\int_{\Gamma}\left(\nabla\psi_0\right)\boldsymbol{H}\cdot{\rm d}\boldsymbol{l}, \end{aligned} \tag{1}$$

where $S_{\rm lit}$ denotes the lit portion of the surface; Γ is the boundary of the lit regions and the shadow regions; $\boldsymbol{E}$ and $\boldsymbol{H}$ are the total electric field and the total magnetic field in dS, respectively; and ψ_0 is the free space Green function

$$\psi_0=\frac{\exp\left({\rm j}k\left|\boldsymbol{r}-\boldsymbol{r}'\right|\right)}{4\pi\left|\boldsymbol{r}-\boldsymbol{r}'\right|}. \tag{2}$$

In far field conditions, the observation point is far away from the source points, so the following approximations are taken.

1) The unit incident wave vector $\hat{\boldsymbol{k}}_{\rm i}$ is directed towards the origin of the centroid coordinate and the unit scattering direction vector $\hat{\boldsymbol{k}}_{\rm s}$ is parallel to the observation point $\boldsymbol{r}'$.

2) The antenna electric field radiation intensity of every facet in the lit regions is equal and the scattered power contributed by each single facet is equal.

3) The Green function may be approximated as follows:

(i) $|\boldsymbol{r}|=r$, $|\boldsymbol{r}'|=r'$, and $r\gg r'$, so the amplitude term can be simplified as $|\boldsymbol{r}-\boldsymbol{r}'|\approx r$.

(ii) As is well known, the scattered field is more sensitive to change of phase, so higher accuracy is required in its approximation. By using a Taylor series, the phase term is expressed as

$$\left|\boldsymbol{r}-\boldsymbol{r}'\right|=r-\hat{\boldsymbol{r}}\cdot\boldsymbol{r}'+o\left(1/r\right). \tag{3}$$

Discarding terms $o(1/r)$ in the series, the Green function is written as

$$\psi_0=\frac{\exp\left({\rm j}k\left|\boldsymbol{r}-\boldsymbol{r}'\right|\right)}{4\pi\left|\boldsymbol{r}-\boldsymbol{r}'\right|}\approx\frac{\exp\left({\rm j}k\left(r-\hat{\boldsymbol{r}}\cdot\boldsymbol{r}'\right)\right)}{4\pi r}. \tag{4}$$

The corresponding gradient of the Green function is approximated as[15]

$$\nabla\psi_0\approx{\rm j}k\hat{\boldsymbol{r}}\psi_0=\frac{{\rm j}k\exp\left({\rm j}kr\right)}{r}\hat{\boldsymbol{r}}\exp\left(-{\rm j}k\left(\hat{\boldsymbol{r}}\cdot\boldsymbol{r}'\right)\right). \tag{5}$$

Only in the far field, such as $r\to\infty$ or $r'\to 0$ for finite r, can the phase approximation of the proposed simplification be qualified. According to the criterion presented in Ref. [16], a maximum phase error is given by $\nabla\varphi=\pi/8$ rad, and the acceptable minimum observation range $r_{\rm ff}$ is estimated using

$$r_{\rm ff}=2D^2/\lambda, \tag{6}$$

where λ is the wave number. $r_{\rm ff}$ is thus proportional to the square of $\max(r')$. In other words, the accuracy of the simplified Green function decreases with increasing r' for a given observation point.

Based on the presented approximations, equation (1) can be simplified as

$$\begin{aligned}\boldsymbol{E}_{\rm s}(\boldsymbol{r}) = & \frac{{\rm j}k\exp\left({\rm j}kr\right)}{4\pi r}\int_{S_{\rm lit}}\hat{\boldsymbol{s}}\left[\left(\hat{\boldsymbol{n}}\times\boldsymbol{E}\right)\right.\\ & \left.-Z_0\hat{\boldsymbol{s}}\times\left(\hat{\boldsymbol{n}}\times\boldsymbol{H}\right)\right]{\rm e}^{{\rm j}k\boldsymbol{r}'\cdot\left(\hat{\boldsymbol{i}}-\hat{\boldsymbol{s}}\right)}{\rm d}s. \end{aligned} \tag{7}$$

3. Near field scattering prediction

In this section, an MPO algorithm is described to compute the near field scattering. Corresponding to the three assumptions proposed in the far field, more accurate approximations are exploited and refined formulations qualified for near field calculations are derived.

3.1. Near field wave propagation

In the near field, the incident wave cannot be treated as a plane wave like as it is in far field conditions and each meshed facet has its own individual incident electric field $\boldsymbol{E}_{\rm i}$ and distinct wave propagation vector $\hat{\boldsymbol{k}}_{\rm i}$ towards its own facet center. In this case, every facet can be seen as a single object with much smaller $\max(r')$ if the surface is meshed densely enough. Therefore the accuracy of the PO can be qualified in a much shorter range. A local reference coordinate system ($x_{\rm c}$, $y_{\rm c}$, $z_{\rm c}$) for each facet is set up with origin located at the center of the facet and unit vector $\hat{\boldsymbol{x}}_{\rm c}$, $\hat{\boldsymbol{y}}_{\rm c}$, $\hat{\boldsymbol{z}}_{\rm c}$ being parallel to $\hat{\boldsymbol{x}}$, $\hat{\boldsymbol{y}}$, $\hat{\boldsymbol{z}}$ of the barycentric coordinate. Then, for the m-th facet, its distinct wave propagation vector $\hat{\boldsymbol{k}}_{{\rm i}m}$ and incident electric field $\boldsymbol{E}_{{\rm i}m}$ are defined as

$$\hat{\boldsymbol{k}}_{{\rm i}m}=\frac{\boldsymbol{R}_{{\rm i}_m}}{\left|\boldsymbol{R}_{{\rm i}m}\right|}=\frac{\boldsymbol{r}'_m-\boldsymbol{r}}{\left|\boldsymbol{r}'_m-\boldsymbol{r}\right|}, \tag{8}$$

$$\boldsymbol{E}_{{\rm i}m}=\boldsymbol{E}_{\rm i}\exp\left(-{\rm j}k\hat{\boldsymbol{k}}_{{\rm i}m}\cdot\boldsymbol{r}'_m\right), \tag{9}$$

where $\boldsymbol{R}_{{\rm i}m}$ is the position vector from the center of the mth facet to the observation point $P(r,\theta,\varphi)$, $\boldsymbol{E}_{\rm i}$ is the incident plane wave vector, and k is the wavenumber.

3.2. Antenna radiation pattern

In the near field, due to partial illumination, the scattered power contributed by each facet is different, and the antenna radiation pattern modulation must be taken into consideration. The real antenna radiation pattern is too complex to be described by a single function, so the Gaussian beam (GB) representation is used in this work as a simplification.

The antenna main beam associated with the GB basis function is given by

$$G_{\mathrm{MB}}(\theta) = \exp\left(-2\ln 2\theta^2/\theta_{\mathrm{B}}^2\right), \quad |\theta| \le \mu, \tag{10}$$

where θ_{B} is the half-power beam width of the mainlobe. μ is the azimuth

$$\mu = \theta_{\mathrm{B}}\sqrt{\ln g_3/(-2\ln 2)}, \tag{11}$$

where g_3 is the gain of the main beam.

The first sidelobe is described by a Gaussian function centered at $\pm 1.5\mu$ as

$$\begin{aligned} G_{\mathrm{B1}}(\theta) &= g_1 \exp\left(-2\ln 2\left(\theta \pm 1.5\mu\right)^2/\theta_{\mathrm{B1}}^2\right), \\ &\mu \le |\theta| \le 2\mu, \end{aligned} \tag{12}$$

where g_1 is the peak gain of the first sidelobe. θ_{B1} is the half-power beam width of the first sidelobe

$$\theta_{\mathrm{B1}} = 0.5\mu\sqrt{(-2\ln 2)/\ln(g_3/g_1)}. \tag{13}$$

Similarly, the second sidelobe centered at $\pm 2.5\mu$ is given by

$$\begin{aligned} G_{\mathrm{B2}}(\theta) &= g_2 \exp\left(-2\ln 2\left(\theta \pm 2.5\mu\right)^2/\theta_{\mathrm{B2}}^2\right), \\ &2\mu < |\theta| \le 3\mu, \end{aligned} \tag{14}$$

where g_2 is the peak gain of the second sidelobe. θ_{B2} is the half-power beam width of the second sidelobe

$$\theta_{\mathrm{B2}} = 0.5\mu\sqrt{(-2\ln 2)/\ln(g_3/g_2)}. \tag{15}$$

Based on the proposed antenna radiation pattern, the scattered power contributed by every single facet can be calculated by examining the intersection angle between the unit vector of the antenna main beam direction and the incident direction.

3.3. Refined simplification of the Green function

The approximation of the Green function is unqualified in the near field. An effective way of overcoming the drawbacks in far field Green function approximation is to resort to a novel simplification. In this work, a refined simplification of the Green function with an arbitrary expansion center is exploited as a substitution.

By introducing an expansion center $\boldsymbol{r}_m$ that lies in the neighborhood of the source point, the $|\boldsymbol{r}-\boldsymbol{r}'|$ in Eq. (2) can be written as

$$R = \left|\boldsymbol{r}-\boldsymbol{r}'\right| = \left|\boldsymbol{r}-\boldsymbol{r}_m-\boldsymbol{r}'+\boldsymbol{r}_m\right| = \left|\boldsymbol{q}-\boldsymbol{q}'\right|, \tag{16}$$

where $\boldsymbol{q} = \boldsymbol{r}-\boldsymbol{r}_m$ and $\boldsymbol{q}' = \boldsymbol{r}'-\boldsymbol{r}_m$.

Only in the condition of $|\boldsymbol{q}| \to \infty$ or $|\boldsymbol{q}'| \to 0$ for finite $|\boldsymbol{q}|$ can the exact behavior be guaranteed. Due to the expansion center $\boldsymbol{r}_m$ lying in the vicinity of the source point $\boldsymbol{r}_m$, when the surface is meshed densely enough, $|\boldsymbol{q}'| = |\boldsymbol{r}-\boldsymbol{r}_m| \to 0$ is satisfied.

The substitution of the near field simplification of the Green function with an arbitrary expansion point $\boldsymbol{r}_m$ used in both magnitude and phase for the approximation in the far field can be given by

$$\psi_0 = \frac{\exp(\mathrm{j}k|\boldsymbol{r}-\boldsymbol{r}'|)}{4\pi|\boldsymbol{r}-\boldsymbol{r}'|} \approx \frac{\exp(\mathrm{j}k\hat{\boldsymbol{\rho}}_{\mathrm{n}}\cdot(\boldsymbol{r}-\boldsymbol{r}'))}{4\pi|\boldsymbol{\rho}_{\mathrm{n}}|}, \tag{17}$$

where the unit vector

$$\hat{\boldsymbol{\rho}}_{\mathrm{n}} = \frac{\boldsymbol{r}-\boldsymbol{r}_m}{|\boldsymbol{r}-\boldsymbol{r}_m|}. \tag{18}$$

The corresponding gradient of the near field Green function is approximated by

$$\begin{aligned} \nabla\psi_0 &\approx \mathrm{j}k\hat{\boldsymbol{\rho}}_{\mathrm{n}}\psi_0 \\ &= \frac{\mathrm{j}k\exp(\mathrm{j}k\hat{\boldsymbol{\rho}}_{\mathrm{n}}\cdot\boldsymbol{r})}{|\boldsymbol{\rho}_{\mathrm{n}}|}\hat{\boldsymbol{\rho}}_{\mathrm{n}}\exp(-\mathrm{j}k(\hat{\boldsymbol{\rho}}_{\mathrm{n}}\cdot\boldsymbol{r}')). \end{aligned} \tag{19}$$

Based on the approximations in near field, equation (1) can be simplified as

$$\begin{aligned} \boldsymbol{E}_{\mathrm{s}}(\boldsymbol{r}) &= \frac{\mathrm{j}k\exp(\mathrm{j}k\hat{\boldsymbol{\rho}}_{\mathrm{n}}\cdot\boldsymbol{r})}{4\pi|\boldsymbol{\rho}_{\mathrm{n}}|}\int_{S_{\mathrm{lit}}}\hat{\boldsymbol{\rho}}_{\mathrm{n}}\big[(\hat{\boldsymbol{n}}\times\boldsymbol{E}) \\ &\quad -Z_0\hat{\boldsymbol{\rho}}_{\mathrm{n}}\times(\hat{\boldsymbol{n}}\times\boldsymbol{H})\big]\mathrm{e}^{\mathrm{j}k\boldsymbol{r}'\cdot\left(\hat{\boldsymbol{i}}-\hat{\boldsymbol{\rho}}_{\mathrm{n}}\right)}\,\mathrm{d}s. \end{aligned} \tag{20}$$

4. Numerical results

In this section, the main performance of the modified algorithm is demonstrated via several representative simulations. The section is divided into two parts. In the first one, the accuracy of the modified physical optics algorithm is verified in both the angle and range. The second part focuses on the variations of the near field scattering characteristics with range, frequency, and azimuth angle. In all the following examples, the structure is illuminated by a vertically polarized wave without special declaration. All of the following calculations are performed on a PC with Quad 3.20 GHz CPUs and 3.94 GB memory.

4.1. Prediction accuracy of modified physical optics

Let us begin with the accuracy analysis of the modified physical optics in far and near field scattering predictions. The results for monostatic RCS of a PEC cylinder with 20 cm diameter and 30 cm length are shown in Fig. 1 for the far field and the near field respectively. Figures 1(a) and 1(b) provide plots of RCS as a function of pitch angle from 0° to 180°. The frequency is 10 GHz.

In Fig. 1(a), the far field RCS by the MPO fits well with the results calculated by the MLFMM in the commercial software FEKO. Figure 1(b) shows the RCS by MPO and measured data[17] at 30% of r_{ff} and an agreement is obtained. It is seen that MPO performs well both in the near and far scattering field calculations. The major error in the calculated results is most probably due to the absence of consideration of edge scattering and creeping waves.

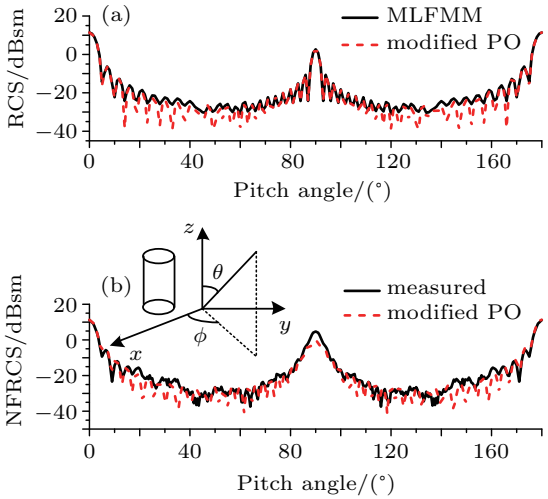


Fig. 1. (color online) The far field monostatic co-polarized RCS of a PEC cylinder with 20 cm diameter and 30 cm length as a function of pitch angle. In (a), the observation is made at $r \gg r_{\rm ff}$. The RCS by MLFMM solution and the MPO solution are presented. In (b), the observation is made at $r = 0.3 \times r_{\rm ff}$. The RCS by measured data[17] and the MPO solution are presented.

The results of the monostatic RCS for a 10 m×10 m square plate varying with range are illustrated in Fig. 2. The frequency is 300 MHz and the observation range varies from 1 m to 10 km in the condition of $\theta = 90°$ and $\varphi = 0°$. In Fig. 2, excellent agreement is obtained between the RCS by MPO and the data in Ref. [18] calculated by the method of moment.

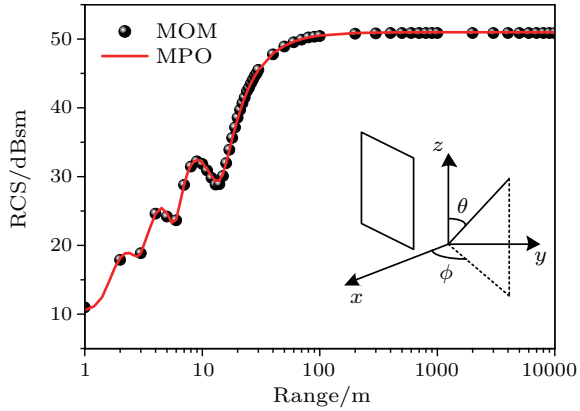


Fig. 2. (color online) The monostatic co-polarized RCS of a $10\lambda \times 10\lambda$ square plate ($\lambda = 1$ m) as a function of observation distance when $\theta = 90°$ and $\varphi = 0°$. The RCS by method of moments solution in Ref. [16] and the MPO solution are presented.

4.2. Near field scattering characteristics of a generic missile

In the following examples, a missile-like target with PEC surface is studied. The size of this target with maximum extent in the rectangular coordinates (x, y, z) are 5.58 m, 2.49 m, and 1.06 m.

Firstly, the computational accuracy and efficiency of the proposed algorithm are studied compared with the very popular MLFMM in FEKO. The results of the monostatic RCS for the generic missile as a function of range are provided in Fig. 3. The frequency is set at 3 GHz for ranges of 10–1000 m. The pitch angle is set at $\theta = 90°$ and $\varphi = 90°$. The computational costs (including RAM and CPU time) for the two solutions are listed in Table 1.

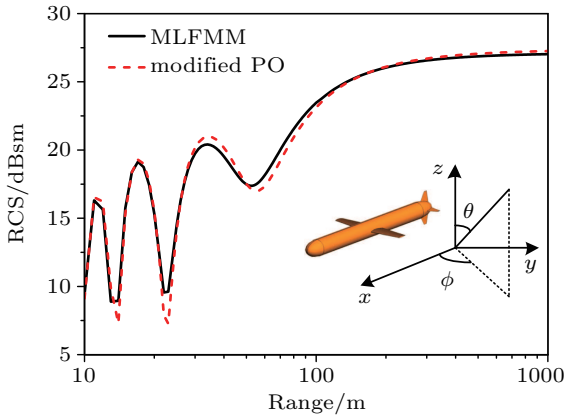


Fig. 3. (color online) The monostatic co-polarized RCS of a missile-like target as a function of observation distance when $\theta = 90°$ and $\varphi = 90°$. The RCS by MLFMM solution in FEKO and the MPO solution are presented.

Table 1. Comparison of the calculation time and memory.

Solution	MLFMM	MPO
Time/s	2223.80	12.91
Memory/MB	5538.21	3.28

As sketched in Fig. 3, the results obtained by MLFMM and MPO have good agreement in most of the distances. The deviation of the plots is most probably due to neglecting edge diffraction and the creeping wave. Besides, it is easy to find from Table 1 that, compared with MLFMM, the MPO solution has a great saving in computing resources.

Next, the RCS of the missile-like target is calculated when viewed from the top ($\varphi = 0°$) and the broadside ($\varphi = 90°$) of the missile. The computed results are shown in Fig. 4 with the frequency set at 1 GHz, 2 GHz, and 3 GHz for ranges of 1–10000 m. The pitch angle is set at $\theta = 90°$.

It is seen that the shake of RCS in near range becomes more violent as the frequency increases. This irregular concussion implies difficulties in near field detection and track. Comparing Figs. 4(a) and 4(b), the near field RCS for $\varphi = 0°$ recovers the far field values at much shorter ranges and the shake of the results is more violent for $\varphi = 90°$. The complex structure and strong specular components of the missile when viewed from the broadside may be responsible for this obvious distinction.

Finally, the results for the monostatic co-polarized RCS of the missile as a function of azimuth angle are calculated. Figure 5 shows the RCS of the missile at 3 GHz in the conditions of far field observation and near field observation at $r = 0.3 \times r_{\rm ff}$. As expected, the two plots presenting far field RCS and near field RCS are different from each other. The variations of the scattered power contributed by single facets and the transference of the dominant scattering centers as the

observation distance changes may be the reason for the difference.

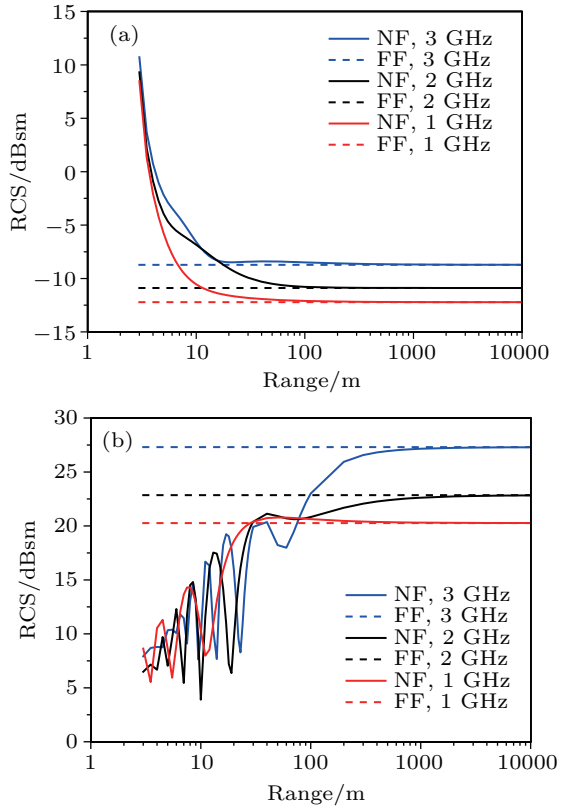


Fig. 4. (color online) The monostatic co-polarized RCS of missile as a function of range when (a) viewed from the top ($\varphi = 0°$) and (b) viewed from the broadside ($\varphi = 90°$). Results are shown for frequencies of 1 GHz, 2 GHz, and 3 GHz. The horizontal dashed lines provide the far field values.

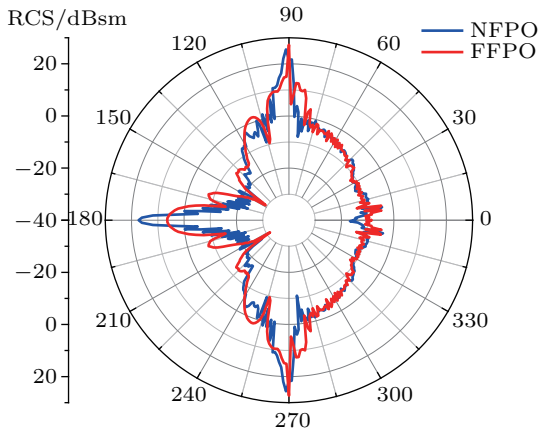


Fig. 5. (color online) The monostatic co-polarized RCS of missile for far field observation (red) and observation at a range of $r = 0.3 \times r_{\mathrm{ff}}$ (blue) as a function of azimuth φ when $\theta = 90°$ and $f = 3$ GHz.

5. Conclusion

An MPO algorithm for scattered field calculation of complex electrically large targets with PEC surfaces for source/observation in the near field and the far field is presented. By setting up local reference coordinates for each facet, the distinct wave propagation vector, the radiation gain based on the modulation of the antenna radiation pattern, and the refined Green function are exploited to adjust the standard PO in the near field scattering calculation. The MPO algorithm retains the accuracy and computational complexities under far field assumptions and performs well both in far field and near field.

Based on the methods proposed, the calculation of near field scattering can be further developed. Future extensions could involve modified equivalent edge currents for edge diffractions and modified iterative physical optics for multiple bounces in cavities.

References

[1] Jeng S 1998 *IEEE Trans. Antennas Propagat.* **46** 551
[2] Neto A 2003 *IEEE Antennas and Propagation Society International Symposium* **4** 416
[3] Chen M, Zhang Y and Liang C H 2005 *J. Elecromagn. Waves Appl.* **19** 1511
[4] Legault S R 2004 *Electron. Lett.* **40** 71
[5] Papkelis E G, Anastassiu H T and Frangos P V 2008 *IEEE Trans. Antennas Propagat.* **56** 3359
[6] Sui M and Xu X J 2010 *IEEE Trans. Antennas Propagat.* **58** 2981
[7] Sui M and Xu X J 2010 2010 *IEEE URSI/APS Symposium*, Toronto
[8] Corucci L, Giusti E, Martorella M and Berizzi F 2012 *IEEE Trans. Antennas Propagat.* **60** 6052
[9] Gendelman A, Brick Y and Boag A 2014 *IEEE Trans. Antennas Propagat.* **62** 4325
[10] Roudstein M, Brick Y and Boag A 2015 *IEEE Trans. Antennas Propagat.* **63** 5015
[11] Cui Y, Chen W, Zhang X and Zheng J 2014 2014 *IEEE International Conference on Computer and Information Technology* 899
[12] Cheng Z, Xie Y and Fan J 2014 *J. Electron. & Inf. Technol.* **36** 1999
[13] Cheng Z, Xie Y, Ma X, Mao Y and Bi B 2015 *J. Electron. & Inf. Technol.* **37** 1002
[14] Guo L X, Wang R and Wu Z S 2010 *Chin. Phys. B* **19** 044102
[15] Wang R, Guo L X and Ma J 2009 *Chin. Phys. B* **18** 3422
[16] Kouyoumjian R G and Peters L 1965 *Proc. IEEE* **53** 920
[17] Côté F 2007 *Simulation de section efficace radar sur une trajectoire* (M.S. thesis) (Quebec City: Laval University)
[18] Legault S R and Louie A 2004 *Validation and implementation of a near-field physical optics formulation* (Technical Memorandum) DRDC Ottawa TM 2004-131, Aug. 2004